Accepted Manuscript

Tectonic strain recorded by magnetic fabrics (AMS) in plutons, including Mt Kinabalu, Borneo: A tool to explore past tectonic regimes and syn-magmatic deformation

A. Burton-Johnson, C.G. Macpherson, J.R. Muraszko, R.J. Harrison, T.A. Jordan

PII: S0191-8141(18)30433-4

DOI: https://doi.org/10.1016/j.jsg.2018.11.014

Reference: SG 3781

To appear in: *Journal of Structural Geology*

Received Date: 23 August 2018

Revised Date: 30 November 2018

Accepted Date: 30 November 2018

Please cite this article as: Burton-Johnson, A., Macpherson, C.G., Muraszko, J.R., Harrison, R.J., Jordan, T.A., Tectonic strain recorded by magnetic fabrics (AMS) in plutons, including Mt Kinabalu, Borneo: A tool to explore past tectonic regimes and syn-magmatic deformation, *Journal of Structural Geology* (2019), doi: https://doi.org/10.1016/j.jsg.2018.11.014.

Tectonic strain recorded by magnetic fabrics (AMS) in plutons, including Mt Kinabalu, Borneo: A tool to explore past tectonic regimes and syn-magmatic deformation

Burton-Johnson, A[a*], Macpherson, C.G.[b], Muraszko, J.R. [c], Harrison, R.J.[c], and Jordan, T.A.[a]

[a]British Antarctic Survey, High Cross, Madingley Road, Cambridge, CB3 0ET, UK

[b]Department of Earth Sciences, University of Durham, Durham, DH1 3LE, UK

[c]Department of Earth Sciences, University of Cambridge, Cambridge, CB2 3EQ, UK

*Author for correspondence

E-mail: alerto@bas.ac.uk

Tel. +44 (0)1223 221284

Keywords: Tectonics; Magnetic fabrics; Magmatic fabrics; Intrusions; Granites; SE Asia; Mt Kinabalu

Highlights

(1) The tectonic fabric in the AMS data of Mt Kinabalu, Borneo, reveals Miocene extension in SE Asia between 7.9-7.3 Ma (later than previously recognised). Correcting for paleomagnetic rotation, extension was oriented NW-SE at 319° ±13.1°.

(2) Tectonic strain fabrics are far more ubiquitous in global plutonic fabrics than previously recognised.

(3) AMS determination of tectonic strain in dated plutons is a powerful tool for determining past tectonics within a temporal framework, particularly when combined with evidence for paleomagnetic rotation.

Abstract

Tectonic strain commonly overprints magmatic fabrics in AMS (Anisotropy of Magnetic Susceptibility) data for plutonic rocks produced by both compressional and extensional regimes. Mt Kinabalu, Borneo, is a composite pluton with an exceptional vertical range of exposure and clearly defined internal contacts. We show that tectonic fabrics are recorded pervasively throughout the intrusion, even near contacts, and present a workflow distinguishing compressive and extensional syn-magmatic deformation. At Mt Kinabalu this reveals a pervasive tectonic fabric indicating NW-SE Miocene extension in Borneo at 7.9-7.3 Ma, later than previously recognised, oriented NW-SE at 319° ±13.1°. Comparing data from Mt Kinabalu with data from globally distributed studies shows that tectonic strain is commonly recorded by plutons. Therefore, AMS fabric can be used to identify the syn-magmatic tectonic setting and combined with both geochronology and evidence for paleomagnetic rotation to provide a powerful tool for accurate determination of syn-magmatic tectonic regimes and strain orientations within temporal frameworks.

1. Introduction

Determining syn-magmatic strain is a challenge for research into plutonic intrusions because traditional structural evidence (faults and dykes) can only record the post-magmatic deformation of their host pluton. Instead, evidence is obtained from mineral fabric alignment (Hutton, 1988; Pitcher, 1997; Paterson et al., 1998; Schofield and D'Lemos, 1998). Be this visible alignment of the rock-forming phases, or more subtle alignment of the magnetically susceptible phases, the recorded strain results from combined magmatic, tectonic, and lithostatic stresses during crystallisation.

Identifying the effects of magmatic or tectonic strain provides valuable information. For example, a magma flow fabric would inform how plutons are intruded, whilst a tectonic fabric would record the tectonic strain orientation during emplacement. However, contrasting interpretations of plutonic mineral fabrics as the recorders of magmatic flow or tectonic strain exist, even for similar intrusions and tectonic settings (e.g. Petronis and O'Driscoll, 2013; Tomek et al., 2016).

In this study we use field and magnetic fabric (AMS, Anisotropy of Magnetic Susceptibility) data from the Mt Kinabalu intrusion of Borneo to demonstrate the pervasive overprint of tectonic fabrics upon magmatic fabrics.. We use the Mt Kinabalu intrusion to demonstrate that determining these tectonic fabrics by AMS offers a powerful tool to obtain temporal constraints on past tectonic regimes. In this case, we constrain the syn-magmatic deformation during a period of disputed tectonics in SE Asia. We compare this with data from other globally distributed plutons to show that such records of deformation are commonly present in granitic plutons,

2. Application of AMS to mineral fabric research

Mineral fabrics in granitic plutons have long been mapped and studied but accurate determinations of these fabrics are often difficult and observations risk being biased by the two dimensional nature of an outcrop. Consequently, analysis of the Anisotropy of Magnetic Susceptibility (AMS) has frequently been applied to granitic intrusions (Bouchez, 1997). This method measures variation

in the susceptibility of each of the three, principal, magnetic axes of an oriented sample (Jezek and Hrouda, 2004); K1, the axis of maximum magnetic susceptibility; K3, the axis of minimum susceptibility; and K2, the intermediate axis (Fig. 1). This method allows fast, inexpensive, and accurate determination of three-dimensional mineral fabrics even when such fabric cannot be observed in outcrop.

Magnetic fabrics can be hosted by ferro-, ferri-, para-, or diamagnetic phases. These classifications and the grain size of the carrier phase determine the nature of observed magnetic fabrics. The magnetic susceptibility of ferro- and ferrimagnetic phases (e.g. magnetite, and pyrrhotite) is three orders of magnitude greater than paramagnetic phases (Hunt et al., 1995). In ferromagnetic minerals all magnetic moments align, whilst in ferrimagnetic minerals some point in the opposite direction. Below their Curie temperature, ferro- and ferrimagnetic phases magnetise when exposed to a magnetic field and remain magnetic once the field is removed. In contrast, the much less magnetic phases exhibiting paramagnetism (e.g. biotite and hornblende) cease being magnetic once the field is removed. The weakest magnetic effect occurs in diamagnetic minerals (e.g. quartz), which are often classed as 'non-magnetic'.

Magnetic domains in ferro- and ferrimagnetic phases cause their magnetic susceptibility to be grain size dependent, with larger grains displaying greater susceptibilities (Hunt et al., 1995). As grain size increases the magnetic domain state changes from single-domain to multi-domain. This is important for AMS studies, as whilst the axes of magnetic susceptibility in multi-domain grains (and the paramagnetic phases biotite and amphibole; Bouchez, 1997) correspond with the grain shape, in single-domain grains the magnetic susceptibility axes are inverted (Stephenson et al., 1986), producing inverse magnetic fabrics (Hrouda and Ježek, 2017). Multi- and single-domain grains can be differentiated by varying the temperature and magnetic field imposed on a sample, as in this study.

3. Development of plutonic mineral fabrics

Magmatic mineral fabrics form during crystallisation in response to the stress experienced by partially molten magma until it cools to its solidus. This stress can be a result of: (1) the primary magma flow during emplacement, including stress applied by the ascending magma column on the melt (e.g. Horsman et al., 2005, Stevenson et al., 2006, Stevenson et al., 2007a, Clemens and Benn, 2010); (2) regional tectonic stress during emplacement and crystallisation (e.g. Vigneresse, 1995, Benn et al., 1997, Benn, 2009); or (3) a combination of both (e.g. Wennerström and Airo, 1998, Petronis et al., 2012). Whether a plutonic mineral fabric (including AMS) records magmatic or tectonic stresses will be determined by the dominating force during final crystallisation of the pluton at the end of its emplacement.

In response to syn-magmatic stress, crystals align their longest principal axis with the long axis of the resultant strain ellipsoid and their shortest principal axis parallel to the short axis of the strain ellipsoid (Fig. 1, Paterson et al., 1998). This relationship of mineral fabric to the strain ellipsoid has been shown by numerical and analogue experiments for simple, non-coaxial shear, for pure, coaxial shear, and for mixed strain conditions (Jeffery, 1922; N. C. Gay, 1968; No C. Gay, 1968; Arbaret et al., 1997; Schulmann et al., 1997; Schulmann and Ježek, 2012).

The relationship between stress and strain is complex and requires consideration, as observed magmatic fabrics may record a spectrum from coaxial to non-coaxial deformation. The resultant AMS fabrics expected for different deformation settings are shown in Fig. 2. Coaxial, non-rotational shear can be expected away from rheological contrasts (i.e. away from internal and external contacts), resulting from tectonic stress, and stress exerted by the upwelling magma and overburden (Paterson et al., 1998).

Under coaxial, non-rotational shear, the shortest principle axis of the strain ellipsoid is parallel to the direction of maximum compressive stress (σ_1, Fig. 1 and Fig. 2) whilst the longest principle axis of the strain ellipsoid will be parallel to the direction of minimum compressive stress (σ_3, Fig. 1 and Fig. 2). The degree to which rigid particles (i.e. the crystal fabric) rotate in response to the strain

ellipsoid will increase at higher degrees of strain (N. C. Gay, 1968), increasing the anisotropy of the fabric. However, assuming a random initial particle distribution, even at low degrees of strain the overall distribution of the respective stress and strain axes (and consequently the AMS fabric) will be parallel; albeit with a lower degree of anisotropy (Arbaret et al., 2000).

Non-coaxial simple, transpressional, and trans-tensional shearing can be expected to affect both magmatic and tectonic fabrics, particularly where there is differential movement near rheological contrasts. This includes both internal and external contacts (Blumenfeld and Bouchez, 1988; Paterson et al., 1998) or where a pluton is emplaced along a shear zone (Archanjo et al., 1999, 2002).

Under non-coaxial shear, with increasing degrees of strain the longest principle axis of the strain ellipsoid (and consequently the crystals) will rotate towards the direction of shearing and consequent stretching (elongation) direction (Fig. 2). The shortest principle axis of the strain ellipsoid and crystals will rotate towards perpendicular to the rheological boundary and orthogonally to the direction of extension (Fig. 2, Arbaret et al., 1997; Benn, 2010). In non-coaxial shear, the relationship between stress and strain orientations is dependent on a number of factors including tectonic setting, the degree of shearing, rheological contrasts and pre-existing structures.

As noted, a crystallising melt will experience a spectrum from coaxial to non-coaxial shearing, complicating derivation of stress and strain vectors. However, coaxial and non-coaxial shear produce distinct and different fabrics (Fig. 2). By predicting these fabrics for the magmatic and tectonic strain regimes of a pluton (Fig. 2) and comparing them with the pluton's observed magmatic fabric, the relative contributions of coaxial and non-coaxial shear can be determined.

4. The Mt Kinabalu Intrusion, Borneo

The Mt Kinabalu intrusion of Sabah, Borneo (Fig. 3), provides an ideal field area to investigate magnetic mineral fabrics in three dimensions across a single composite pluton. This is because it has an extensive, glaciated summit; a 2900m vertical range of granitic exposure; clearly mapped internal and external contacts; and strong temporal constraints on the emplacement historyThe

pluton intruded into the shallow crust (3-12 km, Vogt and Flower, 1989; Cottam et al., 2013; Burton-Johnson et al., 2017) as six major granitic units between 7.85 and 7.55 Ma (Cottam et al., 2010) at the contact between the Mesozoic ophiolitic ultramafic basement (Reinhard and Wenk, 1951; Dhonau and Hutchison, 1965; Koopmans, 1967; Kirk, 1968; Leong, 1974) and overlying Eocene to Lower Miocene turbiditic sandstones of the Crocker Formation (Collenette, 1965; van Hattum et al., 2006). Contrasting geodynamic settings have been proposed for NW Borneo at this time, either as a zone of regional compression (Hutchison, 2000; Swauger et al., 2000; King et al., 2010; Pubellier and Morley, 2013) or regional extension (Cottam et al., 2013; Hall, 2013; Burton-Johnson et al., 2017). Contact metamorphism of the adjacent ultramafic rocks generated talc and anthophyllite, indicative of granitoid emplacement at 630-700°C and 2–3 kbar (7-11 km, Bucher and Grapes, 2011).

Recent work (Cottam et al., 2010; Burton-Johnson et al., 2017) has shown that the composite pluton was initially emplaced from the top down in a broadly laccolithic structure (Fig. 3C) through upward deformation of the host rocks. Consequently, the oldest unit (the Alexandra Tonalite/Granodiorite, 7.85 ±0.08 Ma) overlies the subsequent, larger units (the Low's Granite, 7.69 ±0.07 Ma, and the King Granite, 7.46 ±0.08 Ma). The smaller, vertical planar Donkey Granite (7.49 ±0.03 Ma) intruded the King Granite before the latter could fully crystallise, producing contacts that vary from gradational to mingled. The final two porphyritic units (the Paka Porphyritic Granite, 7.32 ±0.09 Ma, and the Mesilau Porphyritic Granite, 7.22 ±0.07 Ma) deviate from the laccolith model having been emplaced laterally and around the periphery of earlier units (Fig. 3c).

Mineralogies of the units are summarised in Table 1. Petrographically the units are largely classified as granites (Burton-Johnson et al., 2017), although their major element composition is largely granodiorite (Burton-Johnson et al., in review). Hornblende is the dominant mafic phase in all units except the Alexandra Tonalite/Granodiorite, in which biotite dominates. Visible mineral macrofabrics are absent in all units except the Alexandra unit, in which a biotite foliation was observed, dipping ~40-60° towards the south-west (Burton-Johnson et al., 2017). To test this observation, image analysis (adapting the

methodology of Grove and Jerram, 2011) was conducted on thin sections of each unit (Fig. 4), characterising the colour palettes for biotite and hornblende in each section to determine the 2D orientation of the ferromagnesian crystals (Fig. 4). The standardised resultant vector length, $\bar{R}$, (the data distribution parameter in circular directional statistics, Davis 1986) is higher (i.e. more consistently distributed) for the Alexandra unit than the later units for both hornblende (0.008 compared to 0.002) and biotite (0.004 compared to 0.002). Furthermore, no microstructural evidence for shearing was observed in the thin sections of any unit (Fig. 4).

5. Methodology

Whilst the glaciated summit of Mt Kinabalu provides complete exposure, and the topography provides an exceptional vertical range of outcrop, steep cliffs and rainforest-covered flanks limit the area that can be sampled. However, previous work has shown the remarkable lateral homogeneity of AMS fabrics in plutons at a range of scales, with variations in fabric orientations occurring around a mean vector (Bouchez, 1997; Olivier et al., 1997). What is less constrained is the degree AMS fabric heterogeneity vertically through a pluton. The 2900m vertical range of outcrop at Mt Kinabalu provides a unique opportunity to explore this, and consequently sampling focussed on transects to the North, South, East and West of the pluton. Samples were collected at 50m vertical intervals on the summit and the accessible southern flank, and at 100m vertical intervals elsewhere.

94 oriented block samples were collected (Fig. 5) from which 10 to 24 cylindrical cores of $11cm^3$ were drilled per sample at the University of Birmingham, UK (Owens, 1994) The number of cores depended on each sample's weathering and alteration. Oriented cores were analysed on an AGICO KLY-3s Kappabridge at the University of Birmingham to determine the orientation and magnitude (K) of the three principal axes of the AMS fabric (K1, K2 and K3; Fig. 1). Each sub-specimen's results were normalised by the specimen's mean susceptibility (K_{mean}) and averaged for each block sample to determine mean values of the AMS ellipsoid (Jelínek, 1978, Owens, 2000). To determine the magnetic mineralogy,

variability of magnetic susceptibility with temperature was determined on powdered samples at the University of Cambridge, UK. An AGICO MFK1 Kappabridge with a CS4 high temperature attachment and CS-L low temperature attachment was used under an argon atmosphere to reduce secondary oxidation. Samples representing each plutonic unit were selected for detailed magnetic characterisation. Hysteresis loops, DC demagnetisation curves and first-order reversal curve (FORC) diagrams were collected using a Lakeshore Vibrating Sample Magnetometer at the University of Cambridge.

6. Results

6.1. Shape of the AMS fabric

Full results are given in the supplementary material. The shape of the observed AMS fabric is described according to the relative dimensions of the three principal axes of the AMS ellipsoid (Fig. 1). All analysed fabrics lie along a spectrum from purely oblate (a flattened spheroid where K1 = K2 > K3) to purely prolate (an elongated spheroid where K1 > K2 = K3) and are described by the shape parameter, T (Jelinek, 1981) which has a possible range from 1 (purely oblate) to -1 (purely prolate). The degree of measured anisotropy (P', Jelinek, 1981) is used instead of K1/K3 as it refers to deviation of all axes (including K2) from the mean susceptibility. The bulk magnetic susceptibility (K_{Mean}) varies by two orders of magnitude (Fig. 6). The mineral fabric (T) is dominantly oblate (Fig. 6), but for almost all samples the axes are statistically distinct from each other at 95% confidence; allowing statistically valid utilisation of all three axes (including the lineation, K1).

6.2. Magnetic mineralogy

The magnetically susceptible mineralogy can be determined from the variations of magnetic susceptibility with temperature (Fig. 7), hysteresis loops (Fig. 8) and First Order Reversal Curves (FORC diagrams, Fig. 8). All samples except the Alexandra Tonalite/Granodiorite show abrupt reductions in bulk susceptibility on heating between 565-585°C, the Curie temperature of pure magnetite. Although a small Hopkinson peak prior to the 565-585°C reduction in magnetic susceptibility appears to be present in some samples (Fig. 7), the lack of an

extreme peak indicates dominance of multi-domain rather than single or pseudo single-domain particles (Orlický, 1990). The susceptibility decrease at 320-420°C results from the conversion of maghemitised magnetite to hematite (Orlický, 1990), an interpretation supported by the absence of this feature in the cooling curves. For all samples the cooling curve has a higher susceptibility than the heating curve, indicating production of secondary magnetite during heating.

The low bulk susceptibility of the Alexandra Tonalite/Granodiorite indicates a paramagnetic carrier phase, most probably biotite and/or amphibole, given the mineralogy of this unit (Burton-Johnson et al., 2017). This is consistent with the parabolic decease in susceptibility at low temperature (Fig. 7) with no increase at -148°C (the Verwey transition; Walz 2002), indicating that magnetite is not the dominant carrier. The hysteresis loops have a high contribution from paramagnetic minerals, which were corrected for in the analysis (Fig. 8). The samples have low coercivity values in the range of 2.7-8.5 mT, consistent for multi-domain grains (see supplementary material for full results). FORC diagrams for the Alexandra Tonalite/Granodiorite and King Granite (Fig. 8) show low coercivity (B_c) and a wide range in the bias field (B_u), with a weakly expressed negative bias region present on the right hand side of the lobe. These features all indicate multi-domain behaviour, as even small proportions of single-domain grains produce the high coercivity and narrow bias range associated with single-domain behaviour (Fig. 8; Harrison et al., 2018). As the magnetic fabric is and hosted by multi-domain magnetite, biotite, and amphibole, the AMS data does not represent an inverse fabric (as would be produced by single-domain magnetite; Stephenson et al., 1986).

6.3. AMS fabric of the different units

Overall the fabrics of most Mt Kinabalu granitic units display lineation with a shallow, NW plunge (K1; Fig. 9), and shallow dipping foliation (to which K3 is the pole; Fig. 8), although there are deviations. In the Alexandra Tonalite/Granodiorite, lineation of the AMS fabric (K1) shows a shallow plunge to the NW whilst the foliation (K3) has a consistent moderate dip to the SW (Fig. 9). Lineation of the Low's Granite also plunges to the NW but the foliation dip is shallower than the Alexandra unit (Fig. 9). The most sampled unit, the King

Granite, has the most homogenous AMS fabric with a lineation consistently plunging sub-horizontally to the NW/SE and a foliation recording a very shallow SW dip (Fig. 9). The Donkey Granite has the lowest areal extent and thus the fewest samples. Its lineation is variable and dominantly contact-parallel (Fig. 9) while the foliation has a shallow west dip (Fig. 9), although it frequently strikes sub-parallel to the contacts (Fig. 5). The AMS fabric of the Paka Porphyritic Granite again has a shallow NW plunge to its lineation and a shallow west dip to its foliation (Fig. 9). However, deviations in both the lineation and foliation are evident at the eastern extent and near internal contacts (Fig. 5). We obtained relatively few measurements of the Mesilau Porphyritic Granite due to the poor accessibility of the lower forested flanks of Mt Kinabalu. AMS measurements of Mesilau are highly variable in both foliation and lineation (Fig. 9). Thin section examinations of this unit reveal accumulations of secondary hydrothermal magnetite within its fractures and along grain boundaries, leading to the poorly defined AMS fabric (Fig. 9) and largest range of bulk susceptibility (Fig. 6).

7. Discussion

7.1. Tectonic or magmatic fabric?

The AMS fabric of Mt Kinabalu shows clear and consistent orientations through most units but to understand the origin of this fabric we must determine if it represents magmatic or tectonic strain. This distinction is achieved by comparing the AMS fabric with field evidence for tectonic strain (Paterson et al., 1998). Burton-Johnson et al. (2017) investigated the orientations and relationship of several, early, post-magmatic strain indicators in and around Mt. Kinabalu, including orientations of faults, aplite dykes and mafic dykes within the pluton. These indicate a post-magmatic sub-vertical principal compressive stress, σ_1 (i.e. lithostatic pressure), whilst the minimum compressive stress, σ_3, was sub-horizontally NNW-SSE oriented (Fig. 10). This extensional regime contrasts with the NW-SE to N-S striking compressive folds and associated thrust faults of the local sedimentary country rocks (Jacobson, 1970; Burton-Johnson et al., 2017), which record the Early Miocene Sabah Orogeny (Hutchison, 1996) that pre-dates the intrusion.

Under coaxial shear, the extensional stress field recorded by the faults and dykes of the pluton (Fig. 10) would be predicted to generate AMS fabrics with shallow NNW-SSE plunging lineations (K1) and sub-vertically dipping poles to the foliations (K3); similar to Fig. 2c. Fig. 10 shows that this is precisely the syn-magmatic AMS fabric demonstrated by all units except the Donkey Granite and the Mesilau Porphyritic Granite (a result of secondary magnetite), indicating similar syn- and post-magmatic stress regimes. The similarity in the predicted directions of extension from both the field and AMS evidence requires agreement between the principal stress and strain vectors, indicating the dominance of coaxial, non-rotational shear rather than non-coaxial simple shear in the development of the AMS fabric (Fig. 2).

As discussed above, the crystallisation of secondary magnetite in the Mesilau Porphyritic Granite has compromised its magnetic record. The foliation of the Donkey Granite shows shallow dips (Fig. 9), however its lineations tend towards contact-parallel orientations rather than the expected fabric. This orientation of contact-parallel lineation and shallow foliation is generated in dykes through post-flow compaction of a contact-parallel magmatic fabric (Park et al., 1988; Ernst and Baragar, 1992), indicating that the deviation of the Donkey Granite fabric from the overall distribution results from the narrow width of this unit (Burton-Johnson et al., 2017).

7.2. Effect of contacts on tectonic AMS fabrics

The mechanical contrast along internal or external contacts will generate contact-parallel fabrics in plutons. Simple shear elongation of the fabric will occur in the stretching direction (Fig. 2d, Paterson and Tobisch, 1988; Paterson et al., 1998). We have noted this effect in the narrow Donkey Granite but how far from a contact does this affect AMS fabric in the larger units?

The contact between the King Granite and the later Paka Porphyritic Granite can be traced for over 2km on the south flank of Mt Kinabalu (Fig. 5). Samples from either side of the contact show that the lineation in both units reflects the tectonic overprint even from samples <5m from the contact (Fig. 5c). The foliation is more sensitive to contact-parallel fabrics, with the strike of samples

355 close to the boundary rotated towards the contact but only for samples up to
356 100m from the contact (Fig. 5d). Th presence of a contact-parallel foliation but a
357 tectonic fabric in the lineation indicates rotation about a lineation-parallel zone
358 axis or the development of a variably contact-parallel fabric, subsequently
359 overprinted by invariable extension in the lineation direction.

360 As observed in studies of other intrusions (Bouchez, 1997; Olivier et al., 1997),
361 the AMS fabric of Mt Kinabalu shows remarkable lateral homogeneity across the
362 pluton. The vertical range of exposure at Mt Kinabalu also reveals comparable
363 vertical homogeneity. Overprinting of magmatic fabrics by tectonic strain from
364 coaxial, non-rotational shear is pervasive, even <5m from the contacts and
365 across the entire 2900m vertical range of the intrusion. This implies that
366 plutonic AMS fabrics can be used to determine syn-magmatic tectonic strain
367 even when the geometry of the pluton is unknown.

368 **7.3. Application of the AMS fabric to tectonic interpretation**

369 Excluding the two units for which the tectonic fabric is not recorded (The
370 Donkey Granite and Mesilau Porphyritic Granite), the orientations of the
371 maximum (σ_1) and minimum (σ_3) syn-magmatic tectonic compression directions
372 interpreted from AMS are in close agreement with the field evidence (Fig. 10).
373 However, unlike the syn-magmatic strain recorded by the AMS fabric, because
374 faults and dykes must postdate their host they can only date post-magmatic
375 deformation. The AMS data is also less dispersed, and less ambiguous as its
376 vectors correspond with specific vectors of the strain ellipsoid. As the AMS fabric
377 is hosted by the rock itself, it can be dated directly (unlike most faults and other
378 evidence for paleostrain) allowing determination of the strain ellipsoid at a
379 specific time. This provides a powerful tool for structural and tectonic research.

380 The paleomagnetic rotation of the Mt Kinabalu intrusions since emplacement
381 was determined from granitic samples as 11° anticlockwise (±2.4° at 95%
382 confidence, (Fuller et al., 1991). By correcting the azimuth of the lineation
383 (eigenvector of 308° ±10.7° at 95% confidence, the proxy for the syn-magmatic
384 extension direction) by the paleomagnetic rotation we can determine that at 7.9-
385 7.3 Ma Sabah was undergoing NW-SE crustal extension at 319° ±13.1°. This

supports the presence of a NW-SE oriented extensional regime in Sabah during the Miocene, which may be the result of SE-directed slab rollback during subduction of the Celebes Sea to the SE (Cottam et al., 2013; Hall, 2013). Our findings are not compatible with models invoking contemporaneous tectonic compression in the region (Hutchison, 2000; Swauger et al., 2000; King et al., 2010; Pubellier and Morley, 2013). Emplacement during regional extension is more consistent with a setting affected by slab rollback, which has been proposed between 11-10 Ma (Hall, 2013), although our observations suggest that extension persistent until, at least, 7.5Ma..

7.4. Tectonic overprinting of magmatic AMS fabrics: A widespread phenomenon?

We have shown that extensional tectonics pervasively overprinted the AMS fabric of the Mt Kinabalu intrusion. Where observed elsewhere, similar observations have been utilised to infer local strain partitioning (Archanjo et al., 1992, 2002; Benn, 2010), but can AMS be applied to determine tectonic deformation on a global scale? To investigate whether similar overprinting occurs elsewhere we compiled data from intrusions of varying age and dimensions, and from globally distributed compressional and extensional tectonic regimes (Fig. 11). Whilst not a complete global dataset, this provides a global distribution of plutons from known tectonic settings for which there is comprehensive sample coverage, and includes numerous well-recognised studies (e.g. Mt Stuart, Monte Capanne, Dinkey Creek, and Mono Creek – respectively (Bouillin et al., 1993; de Saint Blanquat and Tikoff, 1997; Cruden, 1999; Benn et al., 2001).. The tectonic settings and orientations of compression or extension are from the literature, with the specific orientation shown in Fig. 11 determined by ourselves as in Fig. 1.

Some of the AMS datasets included in our compilation have already been interpreted as recording a tectonic overprint (e.g. the Shellenbarger and Mt Stuart plutons, USA) whilst others have not (e.g. the Pinto Peak intrusion, USA, and the Monte Capanne intrusion, Italy). However, in all cases a clear and consistent fabric is shown by each intrusion. For each example included in our study the orientation of tectonic strain required to generate each fabric through

418 coaxial shear (as illustrated in Fig. 2) is always in agreement with the
419 contemporaneous tectonic regime of the region (Fig. 11).

420 As with Mt Kinabalu, the close agreement of the AMS fabric vectors and regional
421 tectonic stress directions in both compressional and extensional settings
422 indicates the dominance of coaxial, non-rotational shear rather than simple, non-
423 coaxial shear in pluton-scale AMS fabrics. This allows simple interpretation of
424 the stress and strain vectors. Even in plutons associated with major shear zones,
425 field studies have shown that simple shear is only pervasive close to the shear
426 zone (Gleizes et al., 2001; Tikoff et al., 2005; Benn, 2010), returning to more
427 homogenous, coaxial, non-rotational shear fabrics at greater distances from the
428 shear zone; as observed near the contacts of Mt Kinabalu. The pervasiveness of
429 the simple shear regime is dependent on the rheology of the lithology, timing and
430 degree of shearing, and the scale-dependant cooling history of the pluton
431 (Archanjo et al., 2002; Tikoff et al., 2005; Benn, 2010). Where intrusions were
432 metamorphosed and recrystallised in the deeper crust after emplacement, this
433 coaxial tectonic fabric can be imparted millions of years after magmatism
434 (Hrouda et al., 1988; Hrouda and Faryad, 2017).

435 In extensional plutons the lineation direction (K1) is consistently parallel to the
436 azimuth of extension, whilst the foliation dip varies, similar to our observations
437 in the Alexandra Tonalite/Granodiorite of Mt Kinabalu. Similarly, in
438 compressional plutons the pole to foliation (K3) is consistently in the direction of
439 compression whilst the plunge of the lineation varies. In a compressive regime
440 this lineation variation reflects whether σ_2 (Fig. 1) represents lithostatic
441 (vertical) or lateral (tectonic) compression. If σ_2 represents lithostatic
442 compression the lineation will be sub-horizontal but if the degree of tectonic
443 compression is increased and σ_2 becomes horizontal then the lineation will be
444 sub-vertical (Fig. 2a and 2b). Similarly, in an extensional regime the foliation
445 variation reflects the orientation of σ_1 (Fig. 1). If σ_1 represents lithostatic
446 compression the foliation will be sub-horizontal but if the degree of lateral
447 compression increases, and σ_1 becomes horizontal then the foliation dip will be
448 sub-vertical.

Because of these variations in extensional foliation and compressional lineation, comparing the confidence limits of the mean K1 and K3 vectors (Fig. 12) distinguishes whether a pluton was emplaced in a compressive or extensional setting even in the absence of other data (e.g. field evidence for deformation). Using symmetrical 95% confidence angles for the mean spherical vectors of K1 and K3, compressional plutons can be identified at 90% confidence where "K1 confidence angle / K3 confidence angle" <1.2, and extensional plutons can be identified at 90% confidence where "K1 confidence angle / K3 confidence angle" >1.5 (Fig. 12).

We conclude that coaxial tectonic strain is commonly preserved in the AMS fabric of plutonic intrusions. This explains the remarkable homogeneity of AMS fabrics within many individual plutons (Bouchez, 1997; Olivier et al., 1997) and opens up the possibility of using AMS fabrics to determine syn-magmatic deformation. As intrusive magmatism is a common feature of many tectonic settings throughout Earth's history, the nature of a tectonic regime can be investigated from its accompanying plutons. Just like traditional structural evidence, granitic magmatism has long been seen as a product of tectonic deformation (Vigneresse, 1999). By applying this technique, plutons can be used as a potent structural tool for investigating those tectonic processes and identifying tectonic regimes.

8. Conclusions

- The AMS fabric of the Mt Kinabalu intrusion, Borneo, was largely derived by syn-magmatic crustal extension.

- Tectonic strain is highly pervasive throughout the Mt Kinabalu pluton, dominating the AMS foliation to within 100m of contact surfaces, and the AMS lineation to <5m from contact surfaces.

- After paleomagnetic correction for rotation, the AMS data indicates that crustal extension in Sabah at 7.9-7.3 Ma was oriented NW-SE at 319° ±13.1°. This is consistent with other evidence for Late Miocene extension in NW Borneo (Hall, 2013).

- In compressive settings, AMS foliations are consistent but lineations vary. Likewise, in extensional settings, AMS lineations are consistent but foliations vary. Consequently, compressional plutons can be distinguished by the relative scales of the K1 and K3 confidence angles.

- A compilation of global AMS data for intrusions in extensional and compressional regimes reveals the common occurrence of magnetic fabrics preserving tectonic strain. This indicates that the AMS fabrics of plutonic rocks have the potential to be employed globally to determine syn-magmatic tectonic settings.

9. Acknowledgements

This study was funded by the Natural Environment Research Council. We thank Carl Stevenson at the University of Birmingham for providing equipment and training for our AMS analyses and discussion of our results. We wish to thank Robert Hall, Mike Cottam and the SE Asia Research Group at Royal Holloway for their support and discussions throughout this project. We thank Alim Biun, Felix Tongkul and Maklarin Lakim for their assistance in facilitating the field season; Jamili Nais of Sabah Parks who allowed us to work in the National Park; and the mountain guides and researchers of Mt Kinabalu National Park, especially Alijen "Jen", Halli, Jasirin, Sokaibin, Maklarin Lakim, Sapinus, Samuel and Nicholas. We thank Ian Alsop for his work as Editor in reviewing this paper, and an Anonymous reviewer and František Hrouda and for taking the time to review our submission. To receive such a positive review is greatly encouraging.

10. References

Aranguren, a., Cuevas, J., TubIa, J.M., RomAn-Berdiel, T., Casas-Sainz, A., Casas-Ponsati, A., 2003. Granite laccolith emplacement in the Iberian arc: AMS and gravity study of the La Tojiza pluton (NW Spain). Journal of the Geological Society 160, 435–445. https://doi.org/10.1144/0016-764902-079

Arbaret, L., Diot, H., Bouchez, J.L., Lespinasse, P., de Saint-Blanquat, M., 1997. Analogue 3D simple-shear experiments of magmatic biotite subfabrics. Granite: From Segregation of Melt to Emplacement Fabrics. Springer, 129–143.

Arbaret, L., Fernandez, A., Ježek, J., Ildefonse, B., Launeau, P., Diot, H., 2000. Analogue and numerical modelling of shape fabrics: application to strain and flow determination in magmas. Geological Society of America Special Papers 350, 97–109.

Archanjo, C.J., da Silva, E.R., Caby, R., 1999. Magnetic fabric and pluton emplacement in a transpressive shear zone system: the Itaporanga porphyritic granitic pluton (northeast Brazil). Tectonophysics 312, 331–345.

Archanjo, C.J., Olivier, P., Bouchez, J.L., 1992. Plutons granitiques du Seridó (NE du Brésil): écoulement magmatique parallèle à la chaîne révélé par leur anisotropie magnétique. Bull. Sac. Géol. France 163, 509–520.

Archanjo, C.J., Trindade, R.I., Bouchez, J.L., Ernesto, M., 2002. Granite fabrics and regional-scale strain partitioning in the Seridó belt (Borborema Province, NE Brazil). Tectonics 21, 1003.

Benn, K., 2010. Anisotropy of magnetic susceptibility fabrics in syntectonic plutons as tectonic strain markers: the example of the Canso pluton, Meguma Terrane, Nova Scotia. Earth and Environmental Science Transactions of the Royal Society of Edinburgh 100, 147–158. https://doi.org/10.1017/S1755691009016028

Benn, K., Paterson, S.R., Lund, S.P., Pignotta, G.S., Kruse, S., 2001. Magmatic fabrics in batholiths as markers of regional strains and plate kinematics: example of the Cretaceous Mt. Stuart batholith. Physics and Chemistry of the Earth, Part A: Solid Earth and Geodesy 26, 343–354. https://doi.org/10.1016/S1464-1895(01)00064-3

Blumenfeld, P., Bouchez, J.-L., 1988. Shear criteria in granite and migmatite deformed in the magmatic and solid states. Journal of Structural Geology 10, 361–372. https://doi.org/10.1016/0191-8141(88)90014-4

Bouchez, J.L., 1997. Granite is never isotropic: an introduction to AMS studies of granitic rocks. Granite: From Segregation of Melt to Emplacement Fabrics. Springer, 95–112.

Bouillin, J.-P., Bouchez, J.-L., Lespinasse, P., Peˆcher, a., 1993. Granite emplacement in an extensional setting: an AMS study of the magmatic structures of Monte Capanne (Elba, Italy). Earth and Planetary Science Letters 118, 263–279. https://doi.org/10.1016/0012-821X(93)90172-6

Bucher, K., Grapes, R., 2011. Petrogenesis of metamorphic rocks, 8th Edition. ed. Springer, Heidelberg, Germany.

Burton-Johnson, A., Macpherson, C.G., Hall, R., 2017. Internal structure and emplacement mechanism of composite plutons: evidence from Mt Kinabalu, Borneo. Journal of the Geological Society 174, 180–191.

Burton-Johnson, A., Macpherson, C.G., Ottley, C.J., Nowell, G.M., Boyce, A.J., in review. Generation of Mt Kinabalu granite by crustal contamination of intraplate magma modelled by Equilibrated Major Element Assimilation with Fractional Crystallisation (EME-AFC). Journal of Petrology.

Collenette, P., 1965. The geology and mineral resources of the Pensiangan and Upper Kinabatangan area, Sabah. Malaysia Geological Survey Borneo Region, Memoir 12 150.

Cottam, M.A., Hall, R., Sperber, C., Armstrong, R., 2010. Pulsed emplacement of the Mount Kinabalu granite, northern Borneo. Journal of the Geological Society 167, 49–60. https://doi.org/10.1144/0016-76492009-028.Pulsed

Cottam, M.A., Hall, R., Sperber, C., Kohn, B.P., Forster, M.A., Batt, G.E., 2013. Neogene rock uplift and erosion in northern Borneo: evidence from the Kinabalu granite, Mount Kinabalu. Journal of the Geological Society 170, 805–816. https://doi.org/10.1144/jgs2011-130

Cruden, A.R., 1999. Magnetic fabric evidence for conduit-fed emplacement of a tabular intrusion: Dinkey Creek Pluton, central Sierra Nevada batholith, California. Journal of Geophysical Research: Solid Earth 104, 511–530.

Davis, J.C., 1986. Statistics and data analysis in geology, 2nd Edition. ed. Wiley & Sons, New York.

de Saint Blanquat, M., Tikoff, B., 1997. Development of magmatic to solid-state fabrics during syntectonic emplacement of the Mono Creek Granite, Sierra Nevada Batholith. Granite: From Segregation of Melt to Emplacement Fabrics. Springer, 231–252.

Deng, X., Wu, K., Yang, K., 2013. Emplacement and deformation of Shigujian syntectonic granite in central part of the Dabie orogen: Implications for tectonic regime transformation. Science China Earth Sciences 56, 980–992.

Dhonau, T.J., Hutchison, C.S., 1965. The Darvel Bay area, East Sabah, Malaysia. Malaysia Geological Survey Borneo Region, Annual Report for 1965 141–160.

Ernst, R.E., Baragar, W.R.A., 1992. Evidence from magnetic fabric for the flow pattern of magma in the Mackenzie giant radiating dyke swarm. Nature 356, 511.

Fuller, M., Haston, R., Lin, J., Richter, B., 1991. Tertiary paleomagnetism of regions around the South China Sea. Journal of Southeast … 6, 161–184.

Gay, N. C., 1968. The motion of rigid particles embedded in a viscous fluid during pure shear deformation of the fluid. Tectonophysics 5, 81–88.

Gay, No C., 1968. Pure shear and simple shear deformation of inhomogeneous viscous fluids. 1. Theory. Tectonophysics 5, 211–234.

Gleizes, G., Leblanc, D., Olivier, P., Bouchez, J., 2001. Strain partitioning in a pluton during emplacement in transpressional regime: the example of the Néouvielle granite (Pyrenees). International Journal of Earth Sciences 90, 325–340.

Grove, C., Jerram, D.A., 2011. jPOR: An ImageJ macro to quantify total optical porosity from blue-stained thin sections. Computers & Geosciences 37, 1850–1859.

Gutiérrez, F., Payacán, I., Gelman, S.E., Bachmann, O., Parada, M. a., 2013. Late-stage magma flow in a shallow felsic reservoir: Merging the anisotropy of magnetic susceptibility record with numerical simulations in La Gloria Pluton, central Chile. Journal of Geophysical Research: Solid Earth 118, 1984–1998. https://doi.org/10.1002/jgrb.50164

599 Hall, R., 2013. Contraction and extension in northern Borneo driven by subduction
600 rollback. Journal of Asian Earth Sciences 76, 399–411.
601 https://doi.org/10.1016/j.jseaes.2013.04.010
602 Harrison, R.J., Muraszko, J., Heslop, D., Lascu, I., Muxworthy, A.R., Roberts, A.P.,
603 2018. An Improved Algorithm For Unmixing First-Order Reversal Curve
604 Diagrams Using Principal Component Analysis. Geochemistry, Geophysics,
605 Geosystems.
606 Hrouda, F., Faryad, S.W., 2017. Magnetic fabric overprints in multi-deformed
607 polymetamorphic rocks of the Gemeric Unit (Western Carpathians) and its
608 tectonic implications. Tectonophysics 717, 83–98.
609 Hrouda, F., Jacko, S., Hanák, J., 1988. Parallel magnetic fabrics in metamorphic,
610 granitoid and sedimentary rocks of the Branisko and Čierna Hora Mountains
611 (E Slovakia) and their tectonometamorphic control. Physics of the Earth and
612 Planetary Interiors 51, 271–289.
613 Hrouda, F., Ježek, J., 2017. Role of single-domain magnetic particles in creation of
614 inverse magnetic fabrics in volcanic rocks: A mathematical model study.
615 Studia Geophysica et Geodaetica 61, 145–161.
616 Hunt, C.P., Moskowitz, B.M., Banerjee, S.K., 1995. Magnetic properties of rocks and
617 minerals. In: Ahrens, T.J. (Ed.), Rock Physics & Phase Relations: A
618 Handbook of Physical Constants. AGU, Washington D.C., 189–204.
619 Hutchison, C., 2000. A Miocene collisional belt in north Borneo: uplift mechanism
620 and isostatic adjustment quantified by thermochronology. Journal of the
621 Geological Society 157, 783–793.
622 Hutchison, C.S., 1996. The “Rajang accretionary prism” and “Lupar Line” problem of
623 Borneo. Geological Society, London, Special Publications 106, 247–261.
624 https://doi.org/10.1144/GSL.SP.1996.106.01.16
625 Hutton, D.H., 1988. Granite emplacement mechanisms and tectonic controls:
626 inferences from deformation studies. Earth and Environmental Science
627 Transactions of the Royal Society of Edinburgh 79, 245–255.
628 Jacobson, G., 1970. Gunung Kinabalu Area, Sabah, Malaysia. Geological Survey
629 Malaysia, Kuching, Sarawak.
630 Jeffery, G.B., 1922. The motion of ellipsoidal particles immersed in a viscous fluid.
631 Proc. R. Soc. Lond. A 102, 161–179.
632 Jezek, J., Hrouda, F., 2004. Determination of the orientation of magnetic minerals
633 from the anisotropy of magnetic susceptibility. Geological Society, London,
634 Special Publications 238, 9–20.
635 King, R.C., Backé, G., Morley, C.K., Hillis, R.R., Tingay, M.R.P., 2010. Balancing
636 deformation in NW Borneo: Quantifying plate-scale vs. gravitational tectonics
637 in a delta and deepwater fold-thrust belt system. Marine and Petroleum
638 Geology 27, 238–246. https://doi.org/10.1016/j.marpetgeo.2009.07.008
639 Kirk, H.J.C., 1968. The igneous rocks of Sarawak and Sabah. Geological Survey
640 Borneo Region, Malaysia, Bulletin 5, 201.
641 Koopmans, B.N., 1967. Deformation of the metamorphic rocks and the Chert–Spilite
642 Formation in the southern part of the Darvel Bay area, Sabah. Geological
643 Survey of Malaysia, Borneo Region, Bulletin 8, 14–24.
644 Lennox, P.G., de Wall, H., Durney, D.W., 2016. Correlation between magnetic
645 fabrics, strain and biotite microstructure with increasing mylonitisation in the
646 pretectonic Wyangala Granite, Australia. Tectonophysics 676, 170–197.

Leong, K.M., 1974. The geology and mineral resources of the Upper Segama Valley and Darvel Bay area, Sabah, Malaysia. Geological Survey of Malaysia, Memoir 4.

Lin, W., Charles, N., Chen, Y., Chen, K., Faure, M., Wu, L., Wang, F., Li, Q., Wang, J., Wang, Q., 2013. Late Mesozoic compressional to extensional tectonics in the Yiwulüshan massif, NE China and their bearing on the Yinshan–Yanshan orogenic belt: part II: anisotropy of magnetic susceptibility and gravity modeling. Gondwana Research 23, 78–94.

Martins, H.C., Sant'Ovaia, H., Abreu, J., Oliveira, M., Noronha, F., 2011. Emplacement of the Lavadores granite (NW Portugal): U/Pb and AMS results. Comptes Rendus Geoscience 343, 387–396.

Olivier, P., de Saint Blanquat, M., Gleizes, G., Leblanc, D., 1997. Homogeneity of granite fabrics at the metre and dekametre scales. Granite: From Segregation of Melt to Emplacement Fabrics. Springer, 113–127.

Orlický, O., 1990. Detection of magnetic carriers in rocks: results of susceptibility changes in powdered rock samples induced by temperature. Physics of the Earth and Planetary Interiors 63, 66–70.

Otoh, S., Jwa, Y.-J., Nomura, R., Sakai, H., 1999. A preliminary AMS (anisotropy of magnetic susceptibility) study of the Namwon granite, southwest Korea. Geosciences Journal 3, 31–41.

Owens, W.H., 1994. Laboratory drilling of field-orientated block samples. Journal of Structural Geology 16, 1719–1721. https://doi.org/10.1016/0191-8141(94)90137-6

Park, J.K., Tanczyk, E.I., Desbarats, A., 1988. Magnetic fabric and its significance in the 1400 Ma Mealy diabase dykes of Labrador, Canada. Journal of Geophysical Research: Solid Earth 93, 13689–13704.

Paterson, S.R., Fowler, T.K., Schmidt, K.L., Yoshinobu, A.S., Yuan, E.S., Miller, R.B., 1998. Interpreting magmatic fabric patterns in plutons. Lithos 44, 53–82. https://doi.org/10.1016/S0024-4937(98)00022-X

Paterson, S.R., Tobisch, O.T., 1988. Using pluton ages to date regional deformations: problems with commonly used criteria. Geology 16, 1108–1111.

Petronis, M.S., O'Driscoll, B., 2013. Emplacement of the early Miocene Pinto Peak intrusion, Southwest Utah, USA. Geochemistry, Geophysics, Geosystems 14, 5128–5145.

Petronis, M.S., O'Driscoll, B., Stevenson, C.T.E., Reavy, R.J., 2012. Controls on emplacement of the Caledonian Ross of Mull Granite, NW Scotland: Anisotropy of magnetic susceptibility and magmatic and regional structures. Geological Society of America Bulletin 124, 906–927. https://doi.org/10.1130/B30362.1

Pitcher, W.S., 1997. The nature and origin of granite, Second Edition. ed. Chapman & Hall, London, UK.

Pubellier, M., Morley, C.K., 2013. The Basins of Sundaland (SE Asia); evolution and boundary conditions. Marine and Petroleum Geology 58, 555–578.

Reinhard, M., Wenk, E., 1951. Geology of the Colony of North Borneo. British Borneo Geological Survey Bulletin 1.

Sadeghian, M., Bouchez, J.L., Nédélec, a., Siqueira, R., Valizadeh, M.V., 2005. The granite pluton of Zahedan (SE Iran): a petrological and magnetic fabric study of a syntectonic sill emplaced in a transtensional setting. Journal of Asian Earth Sciences 25, 301–327. https://doi.org/10.1016/j.jseaes.2004.03.001

696 Schofield, D.I., D'Lemos, R.S., 1998. Relationships between syn-tectonic granite
697 fabrics and regional PTtd paths: an example from the Gander-Avalon
698 boundary of NE Newfoundland. Journal of Structural Geology 20, 459–471.
699 Schulmann, K., Ježek, J., 2012. Some remarks on fabric overprints and constrictional
700 AMS fabrics in igneous rocks. International Journal of Earth Sciences 101,
701 705–714.
702 Schulmann, K., Jezek, J., Venera, Z., 1997. Perpendicular linear fabrics in granite:
703 markers of combined simple shear and pure shear flows? Granite: From
704 Segregation of Melt to Emplacement Fabrics. Springer, 159–176.
705 Stephenson, A., Sadikun, S. t, Potter, D.K., 1986. A theoretical and experimental
706 comparison of the anisotropies of magnetic susceptibility and remanence in
707 rocks and minerals. Geophysical Journal International 84, 185–200.
708 Swauger, D.A., Hutchison, C.S., Bergman, S.C., Graves, J.E., 2000. Age and
709 emplacement of the Mount Kinabalu pluton. Geological Society of Malaysia
710 Bulletin 44, 159–163.
711 Talbot, J.-Y., Chen, Y., Faure, M., 2005. A magnetic fabric study of the Aigoual–
712 Saint Guiral–Liron granite pluton (French Massif Central) and relationships
713 with its associated dikes. Journal of Geophysical Research 110, B12106–
714 B12106. https://doi.org/10.1029/2005JB003699
715 Tikoff, B., Davis, M.R., Teyssier, C., Blanquat, M. de S., Habert, G., Morgan, S.,
716 2005. Fabric studies within the Cascade Lake shear zone, Sierra Nevada,
717 California. Tectonophysics 400, 209–226.
718 Tomek, F., Žák, J., Verner, K., Holub, F.V., Sláma, J., Paterson, S.R., Memeti, V.,
719 2017. Mineral fabrics in high-level intrusions recording crustal strain and
720 volcano–tectonic interactions: the Shellenbarger pluton, Sierra Nevada,
721 California. Journal of the Geological Society 174, 193–208.
722 Tomek, F., Žák, J., Verner, K., Holub, F.V., Sláma, J., Paterson, S.R., Memeti, V.,
723 2016. Mineral fabrics in high-level intrusions recording crustal strain and
724 volcano–tectonic interactions: the Shellenbarger pluton, Sierra Nevada,
725 California. Journal of the Geological Society jgs2015-151.
726 https://doi.org/10.1144/jgs2015-151
727 van Hattum, M.W., Hall, R., Pickard, A.L., Nichols, G.J., 2006. Southeast Asian
728 sediments not from Asia: Provenance and geochronology of north Borneo
729 sandstones. Geology 34, 589–592.
730 Vigneresse, J.-L., 1999. Should felsic magmas be considered as tectonic objects, just
731 like faults or folds? Journal of Structural Geology 21, 1125–1130.
732 Vogt, E., Flower, M., 1989. Genesis of the Kinabalu (Sabah) granitoid at a
733 subduction-collision junction. Contributions to Mineralogy and Petrology
734 493–509.
735 Walz, F., 2002. The Verwey transition-a topical review. Journal of Physics:
736 Condensed Matter 14, R285.
737 Whitney, D.L., Evans, B.W., 2010. Abbreviations for names of rock-forming
738 minerals. American Mineralogist 95, 185.
739 Wilson, J., 1998. Magnetic susceptibility patterns in a Cordilleran granitoid: the Las
740 Tazas complex, northern Chile. Journal of Geophysical Research: Solid Earth
741 103, 5257–5267.
742

743 **Figure Captions**

744 Fig. 1. Relationship of mineral fabrics (foliation and lineation) and the principal
745 vectors of magnetic susceptibility describing the AMS fabric (K1 – Maximum
746 susceptibility; K2 – Intermediate susceptibility; K3 – Minimum susceptibility) to
747 the strain ellipsoid and the principal stress directions during crystallisation (σ_1 –
748 Maximum compression direction; σ_2. – Intermediate compression direction; σ_3 –
749 Minimum compression direction).

750

751 Fig. 2. Example stereonets (lower hemisphere projection) of the resultant AMS
752 fabrics developed in response to coaxial and non-coaxial strain. Shown are the
753 principal stress directions, simple shear direction, and principal vectors of
754 magnetic susceptibility: K1 – Maximum susceptibility; K2 – Intermediate
755 susceptibility; K3 – Minimum susceptibility.

756

757 Fig. 3. A) Regional geography of Mt Kinabalu and Sabah within SE Asia. B) Aerial
758 photograph of Mt Kinabalu from the south highlighting its extreme vertical relief;
759 courtesy of Tony Barber. C) Internal structure and emplacement ages (Cottam et
760 al., 2010) of the Mt Kinabalu intrusion, as determined from field evidence
761 (Burton-Johnson et al., 2017).

762

763 Fig. 4. Representative thin section images of (a) the Alexandra
764 Tonalite/Granodiorite, and (b) the King Granite (itself representative of the post-
765 Alexandra units). Rose diagrams show the orientations hornblende and biotite
766 crystals in each section. Sections are arbitrarily orientated. Abbreviations as in
767 Fig. 1, plus Hb – Hornblende; Bt – Biotite.

768

769 Fig. 5. Geological map of Mt Kinabalu highlighting the (A) foliation and (B)
770 lineation of the summit plateaux and eastern ridge. Variations in these
771 orientations close to the contact between the King Granite and Paka Porphyritic
772 Granite (box shown in B) are shown in (C) and (D). Abbreviations as in Fig. 5.

773

774 Fig. 6. Relationship of the degree of magnetic anisotropy, P', to the mean bulk
775 susceptibility, K_{Mean} (A), and shape parameter of the AMS fabric, T (B).
776 Abbreviations: Tn – Tonalite, Gd – Granodiorite, Gt – Granite, Pph – Porphyritic
777 Granite.

778

779 Fig. 7. Variation in bulk magnetic susceptibility of each granitic unit with
780 temperature. Abbreviations as in Fig. 5.

781

782 Fig. 8. Hysteresis loops and First Order Reversal curves for: a) the Alexandra
783 Tonalite/Granodiorite; b) the King Granite. The King Granite is representative of
784 the plutons' other composite units. Two synthetic binary mixtures of c) purely
785 multi-domain (MD), and d) a mixture of multi- and single-domain (SD) magnetite
786 are shown for comparison (Harrison et al., 2018).

787

788 Fig. 9. Lower hemisphere projections of the lineation (K1) and pole to the
789 foliation (K3) for the AMS fabric of each of Mt Kinabalu's composite units.
790 Abbreviations as in Fig. 5.

791

792 Fig. 10. Poles to planes for faults, aplite dykes and mafic dykes cross-cutting Mt
793 Kinabalu (Burton-Johnson et al., 2017) compared to lineation (K1) and poles to
794 foliation (K3) of the AMS fabric (excluding the Donkey Granite and Mesilau
795 Porphyritic Granite). Open arrows illustrate the interpreted associated principal
796 stress directions for structural data. Diamonds indicate maximum eigenvectors.

797

798 Fig. 11. Global compilation of lineation (K1) and pole to foliation (K3) directions
799 of AMS data from intrusions emplaced in both extensional and compressive
800 tectonic settings showing the orientation of the principal extensional or
801 compressional direction generating the tectonic fabric.

802 Mt Kinabalu, Borneo – This study; Yiwulüshan massif - Lin et al. (2013);
803 Zahedian - Sadeghian et al. (2005); Monte Capanne - Bouillin et al. (1993);
804 Aigoual–Saint Guiral–Liron - Talbot et al. (2005); La Tojiza - Aranguren et al.
805 (2003); Shigujian - Deng et al. (2013); Ross of Mull - Petronis et al. (2012); Pinto
806 Peak - Petronis and O'Driscoll (2013); Namwon - Otoh et al. (1999); Lavadores -
807 Martins et al. (2011); Las Tazes - Wilson (1998); Wyangala - Lennox et al.
808 (2016); La Gloria - Gutiérrez et al. (2013); Mt Stuart - Benn et al. (2001); Dinky
809 Creek - Cruden (1999); Shellenbarger - Tomek et al. (2017); Mono Creek - de
810 Saint Blanquat and Tikoff (1997).

811

812 Fig. 12. 95% symmetrical confidence limits of the mean spherical K1 and K3
813 vector for the compressional and extensional plutons in Fig. 11. Compressional
814 plutons can be identified at 90% confidence where "K1 95% Confidence Angle /
815 K3 95% Confidence Angle" <1.2, and extensional plutons can be identified at
816 90% confidence where "K1 95% Confidence Angle / K3 95% Confidence Angle"
817 >1.5.

818

819 Table 1. Summary of U-Pb zircon ages (Cottam et al., 2010), SiO_2 and Mg#
820 (Burton-Johnson et al., in review), estimated volumes and modal mineralogies
821 (Burton-Johnson et al., 2017) of the major granitoid units. Abbreviations used:
822 Tn – Tonalite; Gd – Granodiorite; Gt – Granite; Pph – Porphyritic Granite; Qz –
823 Quartz; Pl – Plagioclase; Kfs – Potassium Feldspar; Hb – Hornblende; Bt – Biotite;
824 Cpx. – Clinopyroxene; Ap – Apatite; Ep – Epidote; Zrn – Zircon; Spn – Sphene
825 (Whitney and Evans, 2010).

Unit	Alexandra Tn/Gd	Low's Gt	King Gt	Donkey Gt	Paka Pph	Mesilau Pph
U-Pb Age (Ma)	7.85 ±0.08	7.69 ±0.07 – 7.64 ±0.11	7.46 ±0.08 – 7.44 ±0.09	7.46 > t > 7.32	7.32 ±0.09 – 7.22 ±0.07	–
Approx. Vol. (Km3)	0.2	2 (W) 4 (N)	90	0.4	40	40
SiO2 (wt. %)	61-65	59-64	62-66	63-65	63-67	60-65
Mg#	47-52	50-53	44-53	43-50	44-47	44-47
Phases (Modal %)						
Qz	23-28	16-28	14-27	23	15-21	7-21
Pl	40-45	25-33	21-38	26	23-33	24-28
Kfs	4-7	18-29	26-36	25	23-35	38-48
Hb	4-13	21-28	9-21	11	11-24	8-23
Bt	9-19	4-7	0-5	13	1-2	0-5
Cpx	–	–	–	–	–	0-2
Accessory	Ap, Ep	Ap, Ep, Zrn	Ap, Ep, Zrn	Ap	Ap	Ap, Spn

Table 1. Summary of U-Pb zircon ages (Cottam et al., 2010), SiO2 and Mg# (Burton-Johnson et al., In Review), estimated volumes and modal mineralogies (Burton-Johnson et al., 2017) of the major granitoid units. Abbreviations used: Tn – Tonalite; Gd – Granodiorite; Gt – Granite; Pph – Porphyritic Granite; Qz – Quartz; Pl – Plagioclase; Kfs – Potassium Feldspar; Hb – Hornblende; Bt – Biotite; Cpx. – Clinopyroxene; Ap – Apatite; Ep – Epidote; Zrn – Zircon; Spn – Sphene (Whitney and Evans, 2010).

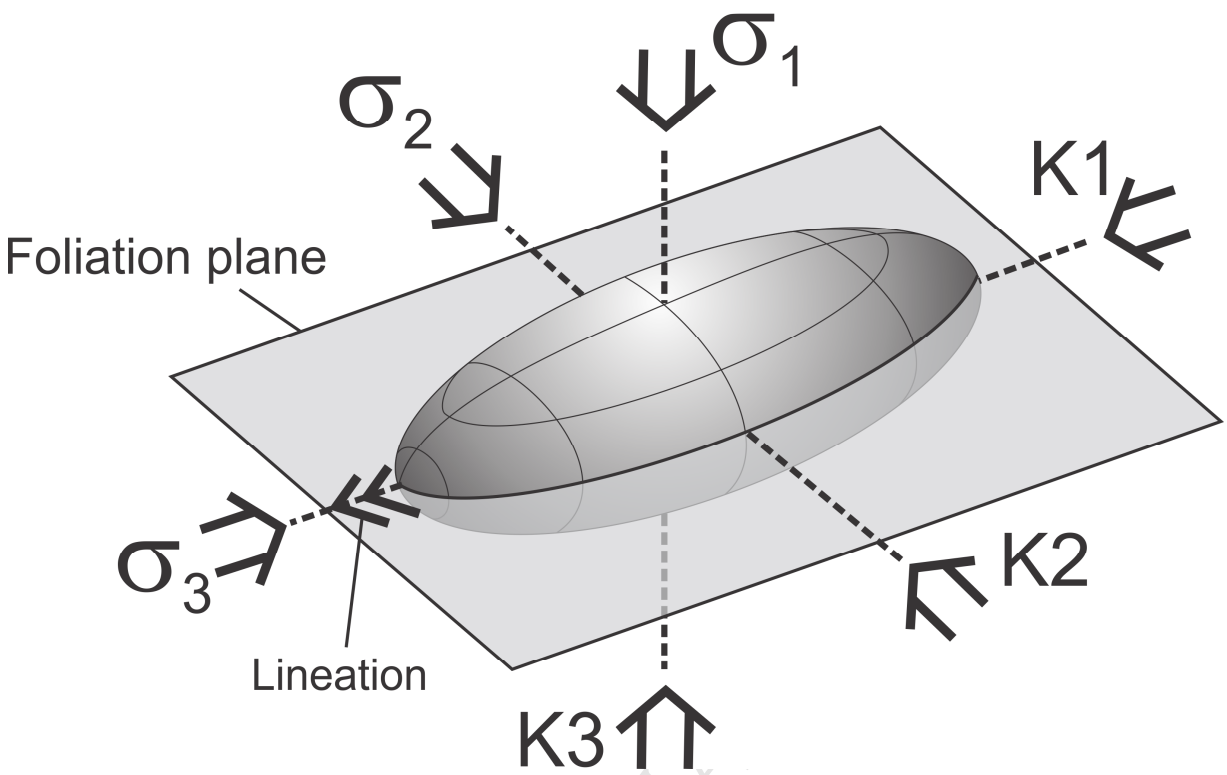

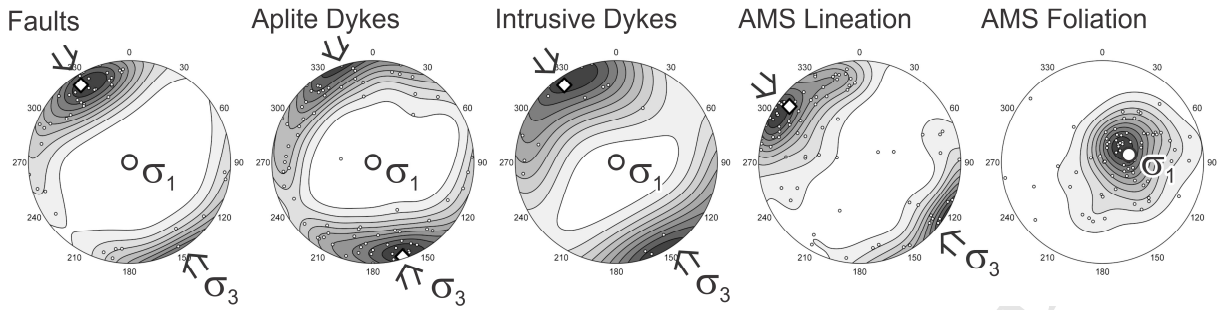

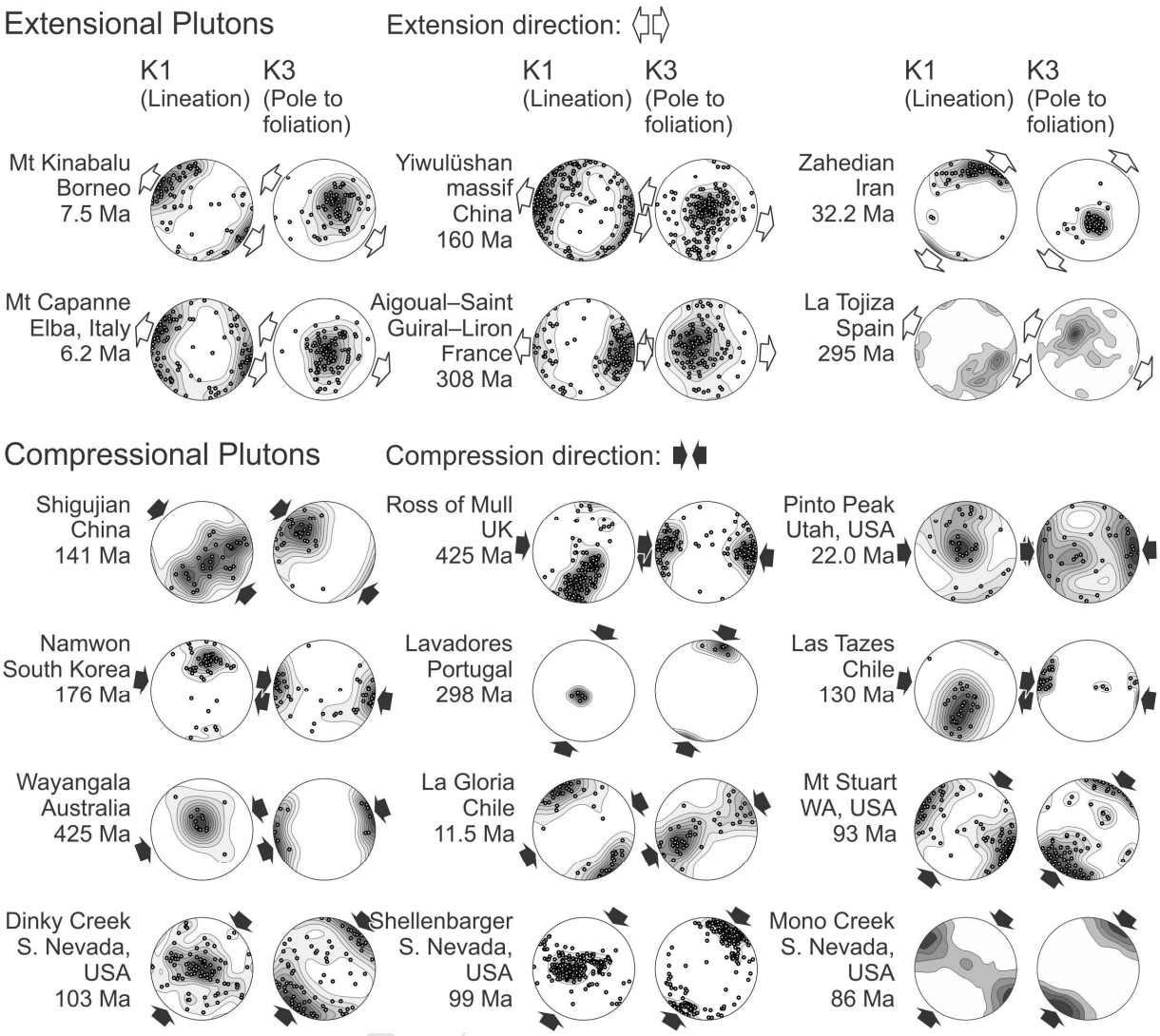
Extensional Plutons
Extension direction:
K1 (Lineation)
K3 (Pole to foliation)
Mt Kinabalu Borneo 7.5 Ma
Yiwulüshan massif China 160 Ma
Zahedian Iran 32.2 Ma
Mt Capanne Elba, Italy 6.2 Ma
Aigoual–Saint Guiral–Liron France 308 Ma
La Tojiza Spain 295 Ma
Compressional Plutons
Compression direction:
Shigujian China 141 Ma
Ross of Mull UK 425 Ma
Pinto Peak Utah, USA 22.0 Ma
Namwon South Korea 176 Ma
Lavadores Portugal 298 Ma
Las Tazes Chile 130 Ma
Wayangala Australia 425 Ma
La Gloria Chile 11.5 Ma
Mt Stuart WA, USA 93 Ma
Dinky Creek S. Nevada, USA 103 Ma
Shellenbarger S. Nevada, USA 99 Ma
Mono Creek S. Nevada, USA 86 Ma

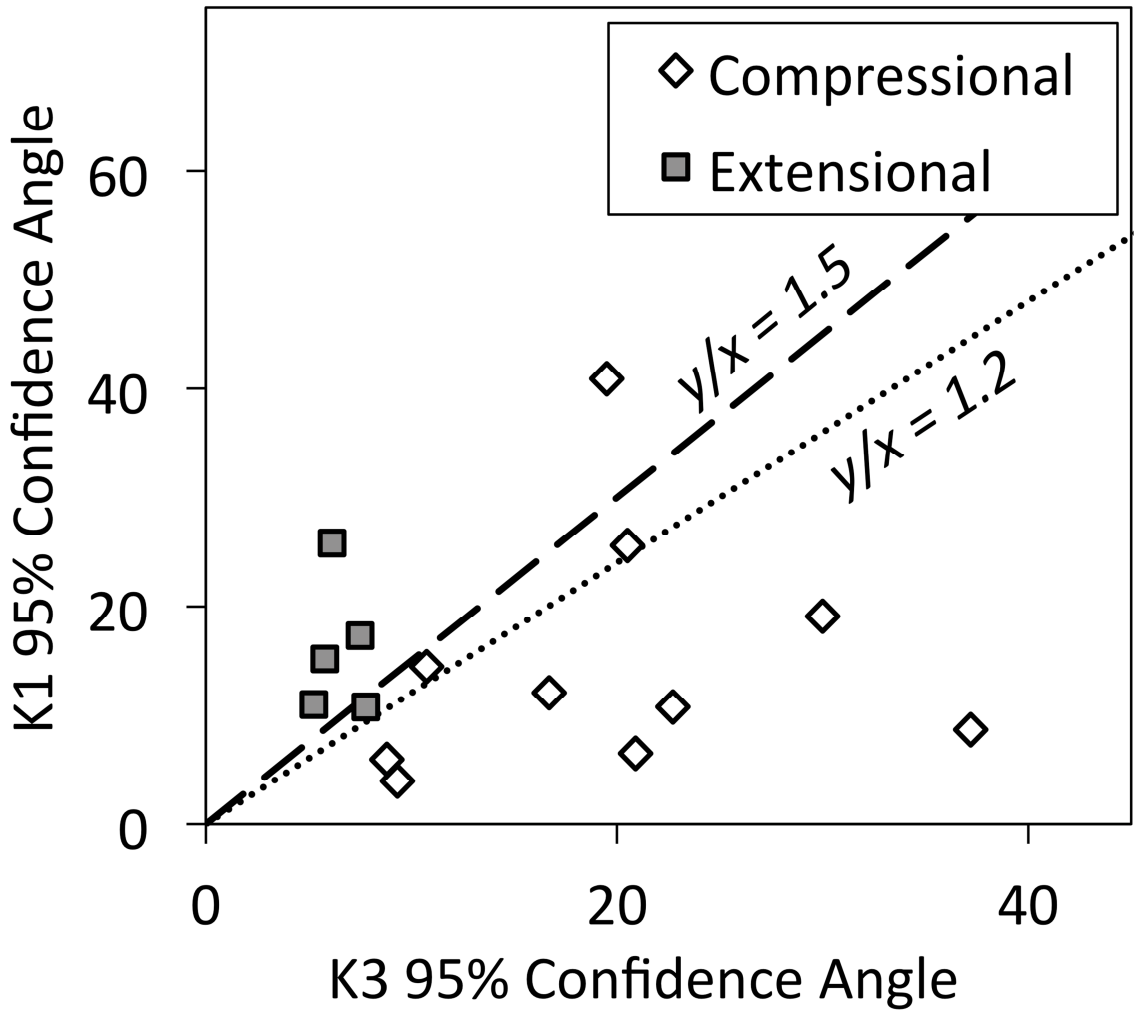

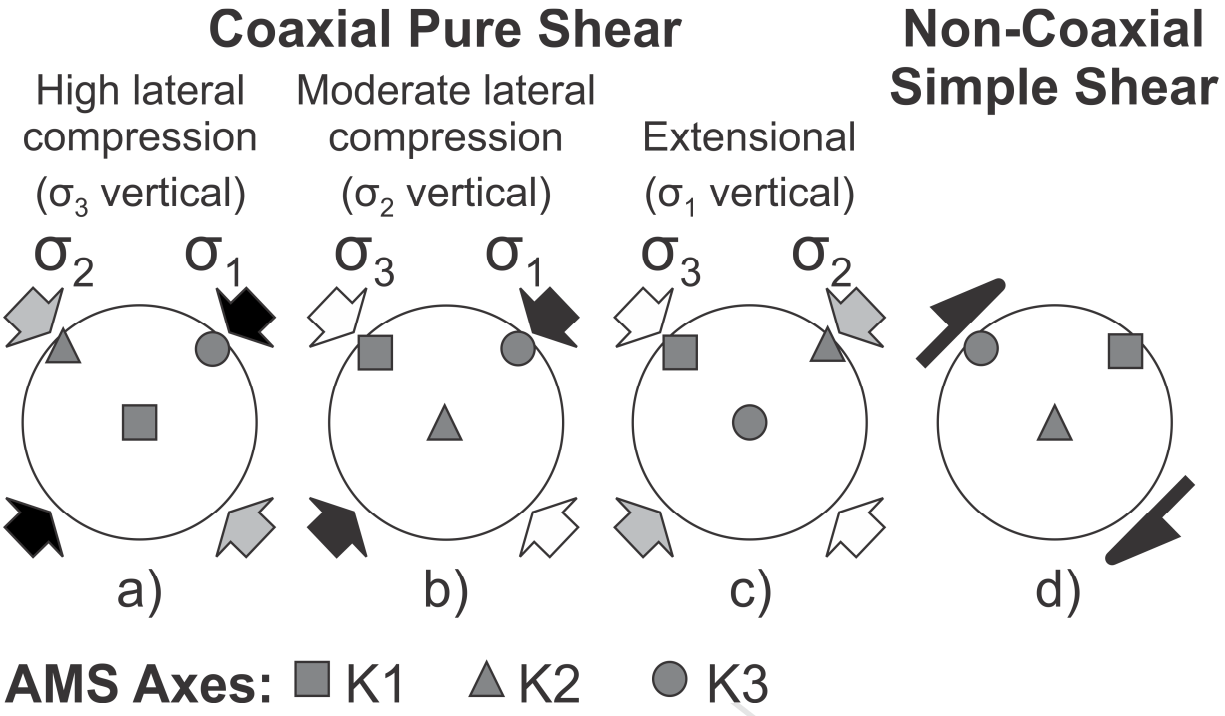

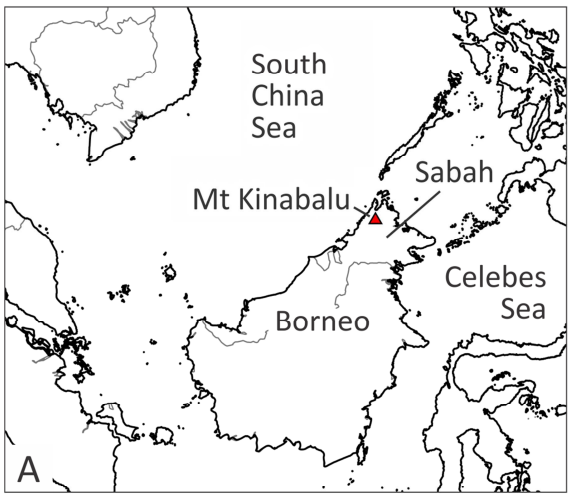
South
China
Sea
Sabah
Mt Kinabalu
Celebes
Sea
Borneo
A


B

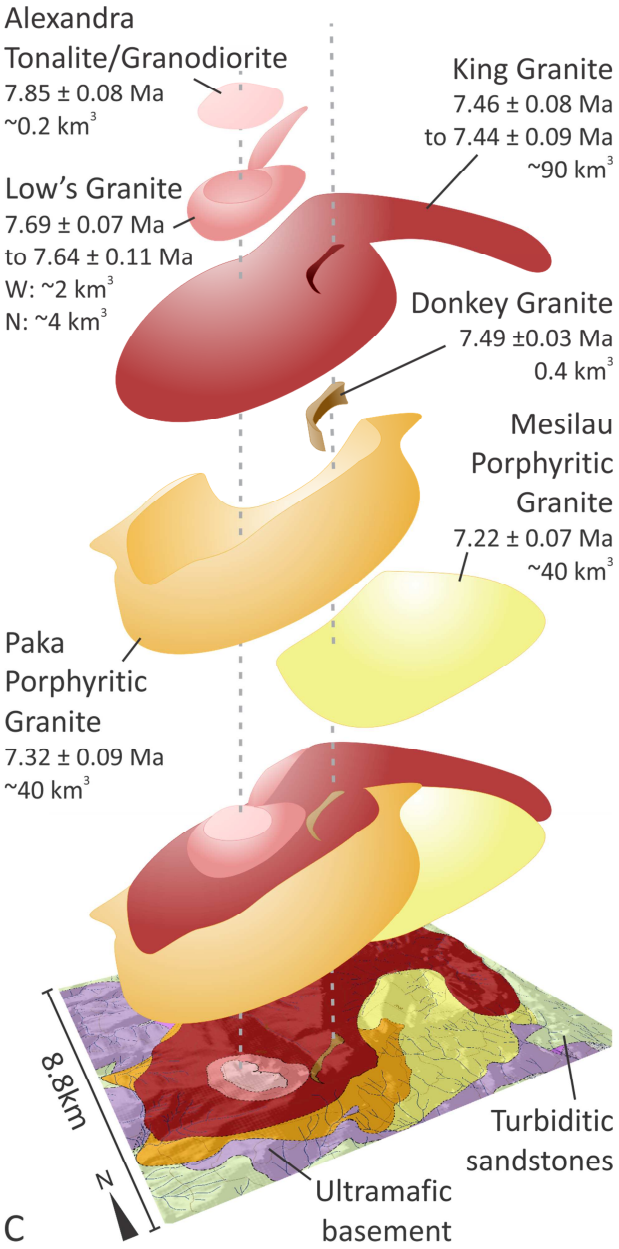
Alexandra
Tonalite/Granodiorite
7.85 ± 0.08 Ma
~0.2 km3
King Granite
7.46 ± 0.08 Ma
to 7.44 ± 0.09 Ma
~90 km3
Low's Granite
7.69 ± 0.07 Ma
to 7.64 ± 0.11 Ma
W: ~2 km3
N: ~4 km3
Donkey Granite
7.49 ±0.03 Ma
0.4 km3
Mesilau
Porphyritic
Granite
7.22 ± 0.07 Ma
~40 km3
Paka
Porphyritic
Granite
7.32 ± 0.09 Ma
~40 km3
8.8km
N
Turbiditic
sandstones
Ultramafic
basement
C

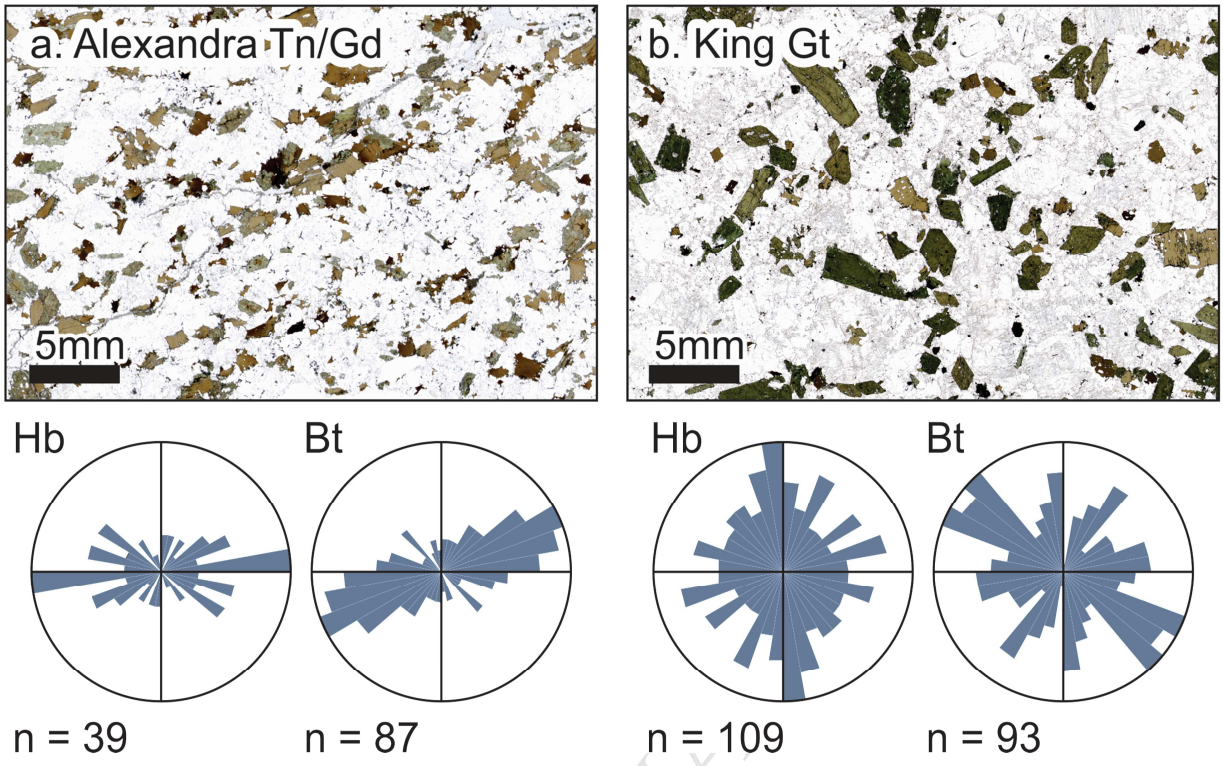

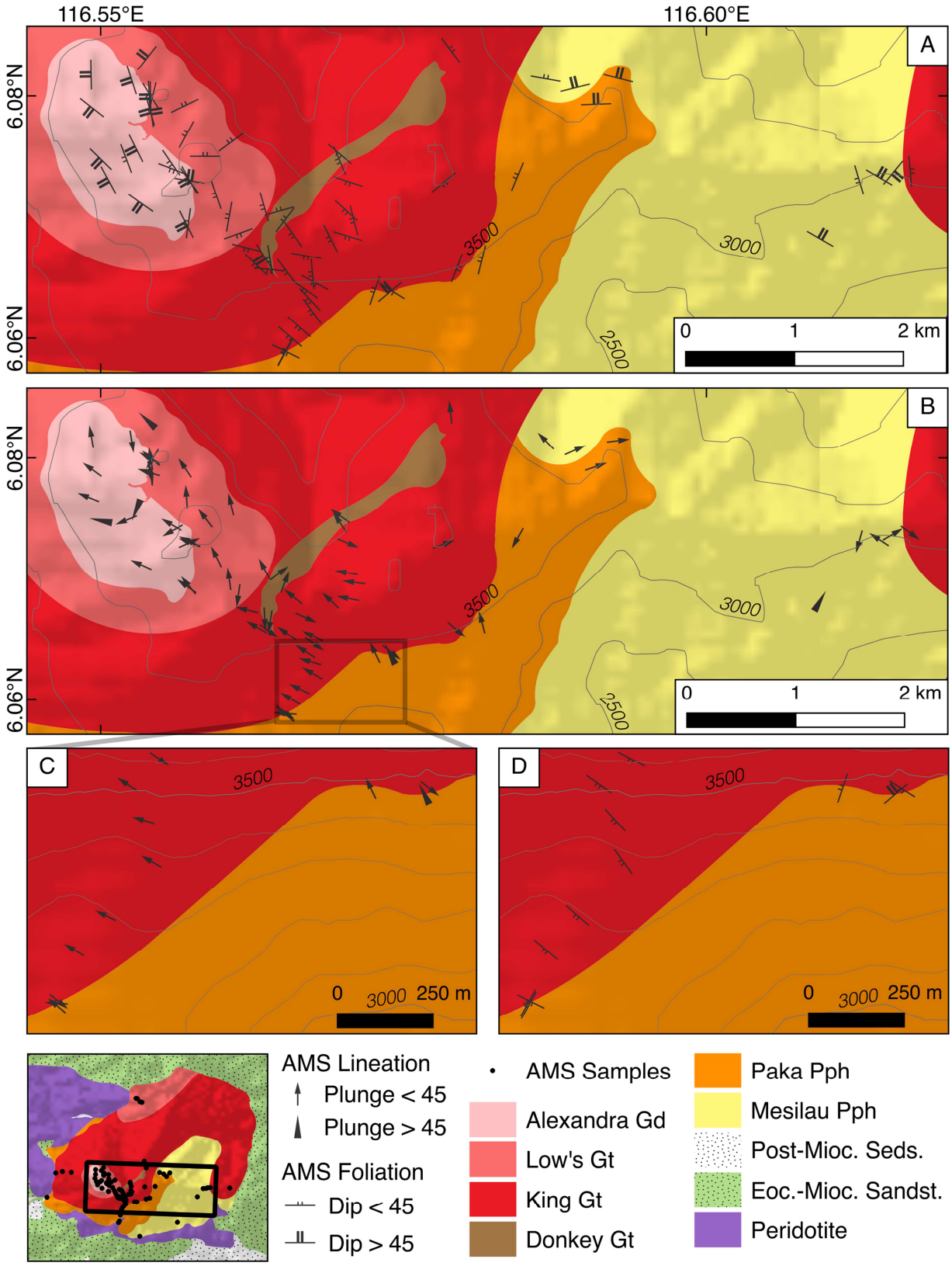
116.55°E
116.60°E
6.08°N
6.06°N
A
B
C
D
3500
3000
2500
0
1
2 km
0
3000
250 m
AMS Lineation
Plunge < 45
Plunge > 45
AMS Foliation
Dip < 45
Dip > 45
AMS Samples
Alexandra Gd
Low's Gt
King Gt
Donkey Gt
Paka Pph
Mesilau Pph
Post-Mioc. Seds.
Eoc.-Mioc. Sandst.
Peridotite

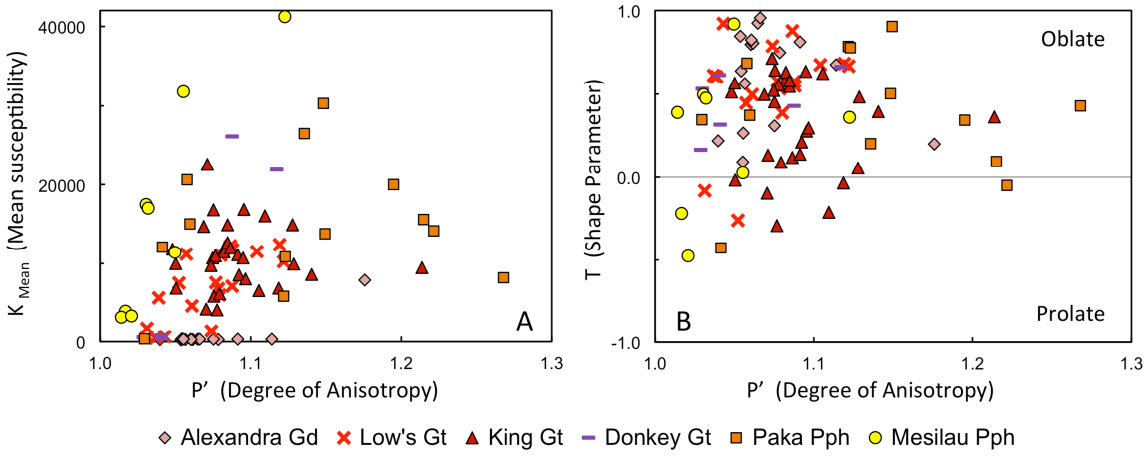
40000
20000
0
K Mean (Mean susceptibility)
1.0
1.1
1.2
1.3
P' (Degree of Anisotropy)
A
1.0
0.0
-1.0
T (Shape Parameter)
Oblate
Prolate
B
Alexandra Gd
Low's Gt
King Gt
Donkey Gt
Paka Pph
Mesilau Pph

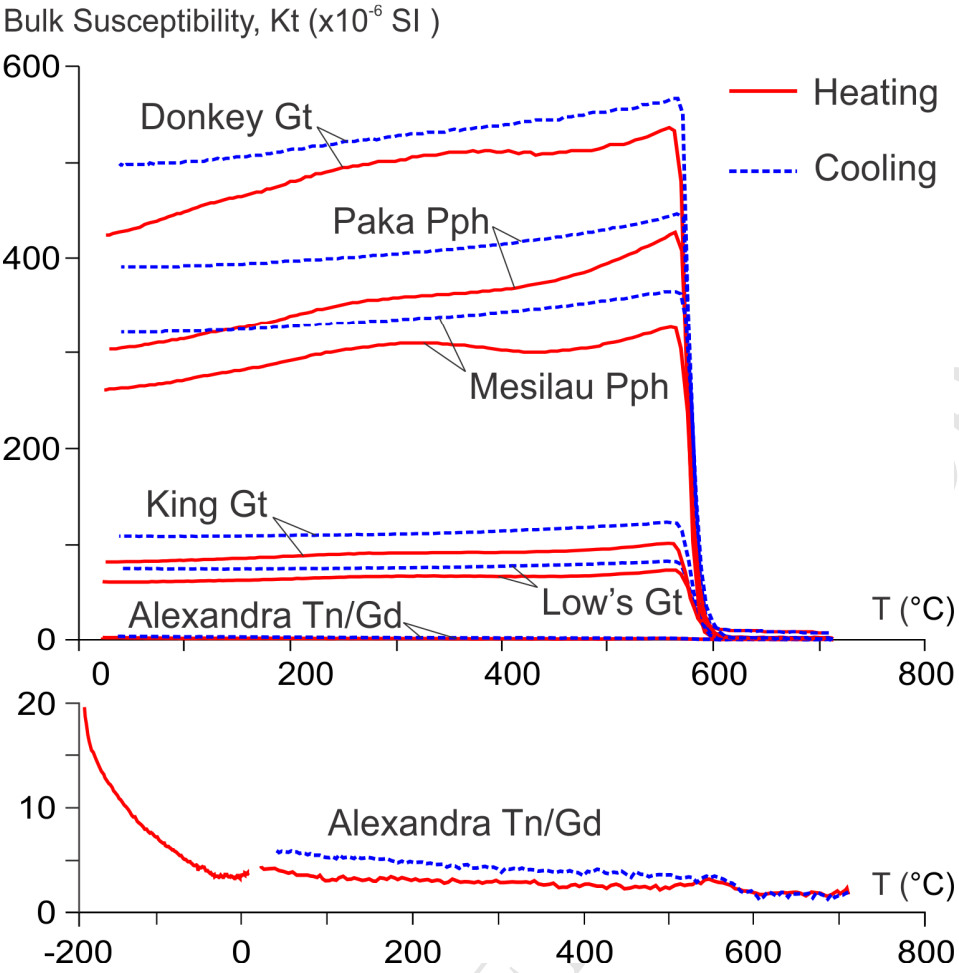

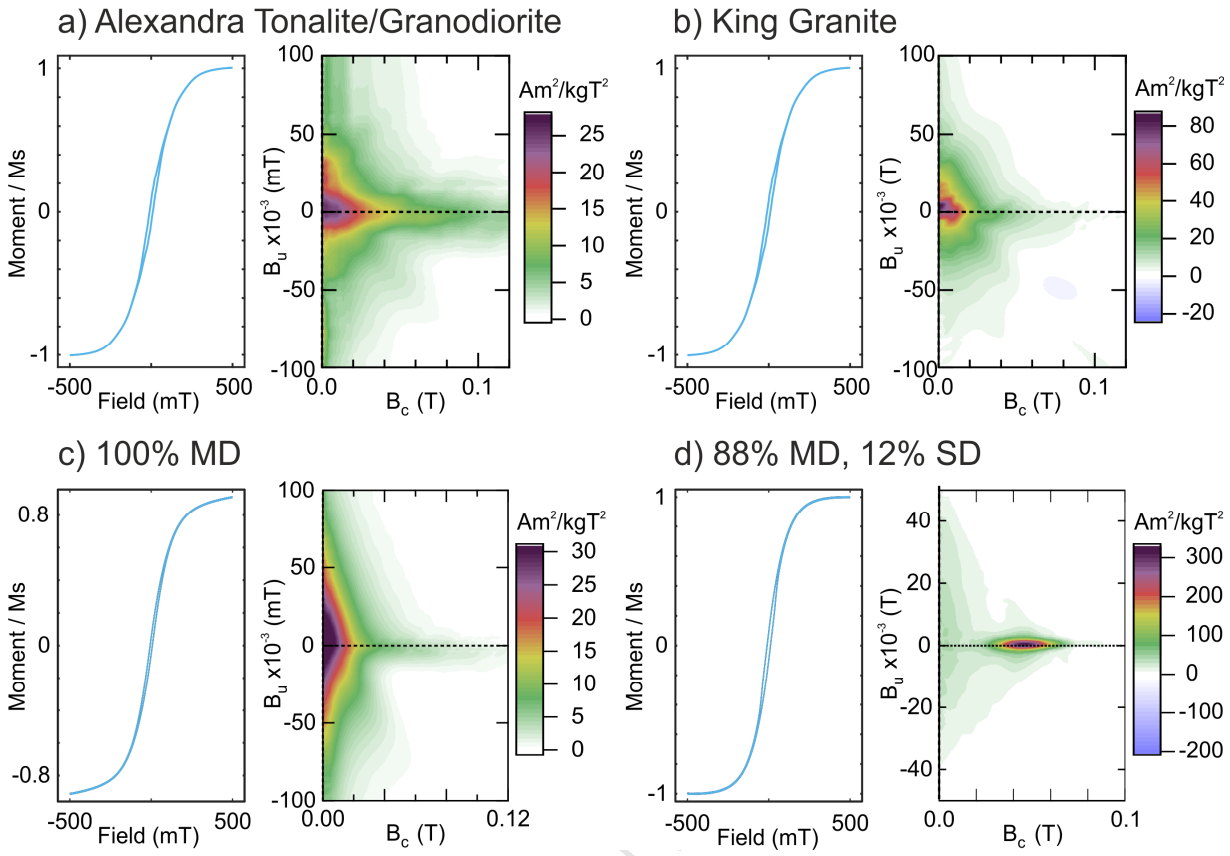

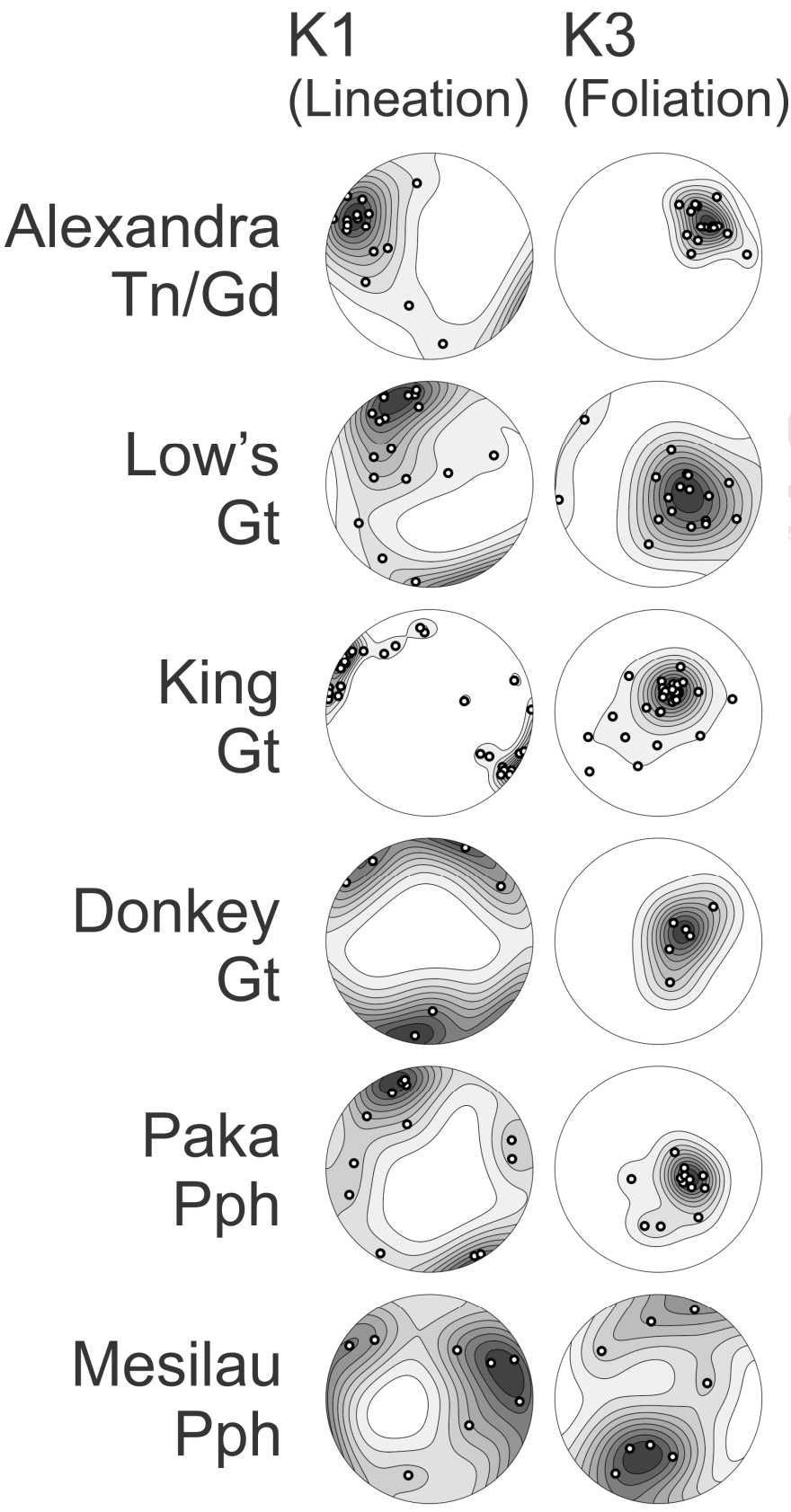
K1
(Lineation)
K3
(Foliation)
Alexandra
Tn/Gd
Low's
Gt
King
Gt
Donkey
Gt
Paka
Pph
Mesilau
Pph